ELSEVIER

www.elsevier.nl/locate/jorganchem

Journal of Organometallic Chemistry 614–615 (2000) 99–106

Journal of Organometallic Chemistry

Synthesis and coordination behavior of a zirconocene bis(borylphosphane)

Tuqiang Chen [a], Eileen N. Duesler [a], Heinrich Nöth [b], Robert T. Paine [a,*]

[a] *Department of Chemistry, Clark Hall 103, University of New Mexico, Albuquerque, NM 87131-1096, USA*
[b] *Department Chemie, Universität München, Butenandtstr. 5-13, D-80333 Munich, Germany*

Dedicated to Professor Sheldon Shore in honor of his 70th birthday.

Abstract

The reaction of $LiP(H)B(N^iPr_2)[N(SiMe_3)_2]\cdot DME$ with Cp_2ZrCl_2 in a 2:1 ratio yields the metallodiphosphane $Cp_2Zr\{P(H)B(N^iPr_2)[N(SiMe_3)_2]\}_2$ (**3a**). Combination of **3a** with $Mo(CO)_4$ (norbornadiene) provides the adduct $Cp_2Zr\{P(H)B(N^iPr_2)[N(SiMe_3)_2]\}_2\cdot Mo(CO)_4$ (**4a**) in which the metallo-diphosphane **3a** acts as a chelating ligand. The compounds have been characterized by spectroscopic methods and the molecular structures of **3a** and **4a** have been determined by single-crystal X-ray diffraction methods. The chemical and structural features are compared and contrasted with related metallo-diphosphanes that contain organic substituents on the diphosphane P atoms. © 2000 Elsevier Science B.V. All rights reserved.

Keywords: Aminoborylphosphanes; Zirconocene; Metal carbonyls

1. Introduction

Primary and secondary monophosphanes, RPH_2 and R_2PH, and diphosphanes, $(H_2P)_2CH_2$, $[R(H)P]_2CH_2$ and $[R(H)P]_2C_2H_4$, containing organic substituents are relatively common, and the use of these compounds as ligands has been extensively studied [1]. On the other hand, primary and secondary phosphanes carrying inorganic substituents, e.g. $(X_nE)PH_2$, $(X_nE)_2PH$, $(X_nE)(Y_mE')PH$ and $[(X_nE)(H)P]_2(EY_m)$ (E = main group element, X, Y = alkyl, aryl, halide, alkoxy, amido) are less common and until recently examples with boryl substituents (E = boron) were especially rare [2]. We are interested in the general aspects of the reactivity of these compounds because they may be useful for the assembly of more complex ring and cage compounds. Indeed, primary and secondary boryl-substituted monophosphanes are in most cases relatively stable, and they have been used as reagents to form more complex phosphanes [2]. The primary diphosphanes, however, tend to readily undergo phosphane elimination chemistry as depicted in Eq. (1) [3]. In one case, the diphosphane $^iPr_2NB(PH_2)_2$ has been trapped and stabilized by coordination with two $Cr(CO)_5$ fragments [4]. However, attempts to form the diphosphane chelate complex $^iPr_2NB(PH_2)_2\cdot Mo(CO)_4$ were unsuccessful. The secondary boryl diphosphane compounds (**2**) are noticeably more stable at 23°C [2,5–7], and they have found use as ligands and as reagents for the formation of more complex compounds. A few examples of silyl bridged boryl diphosphanes **3** have recently been obtained, and one of these compounds (X = Me; $R_2N = {}^iPr_2N$) acts as a chelating diphosphane on a $W(CO)_4$ fragment [8]. This observation led us to attempt the preparation of additional secondary boryl diphosphanes with larger bridging groups, X_2E. Here we report the formation of a zirconocene bis(borylphosphane), $Cp_2Zr\{P(H)B(N^iPr_2)[N(SiMe_3)_2]\}_2$ (**3a**) and its chelation with a $Mo(CO)_4$ fragment.

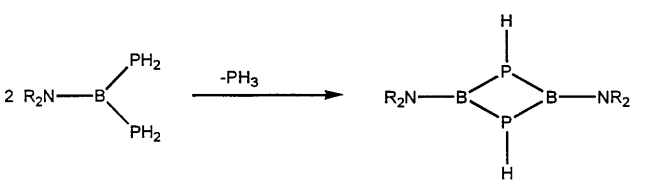

1

$R_2N = {}^iPr_2N$, $(Me_3Si)_2N$, Ph_2N, tmp (1)

* Corresponding author. Tel. +1-505-277-1661; fax: +1-505-277-2609.
E-mail address: rtpaine@unm.edu (R.T. Paine).

PII: S0022-328X(00)00561-1

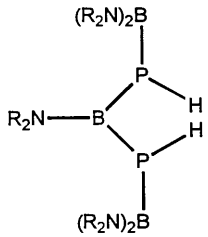

2

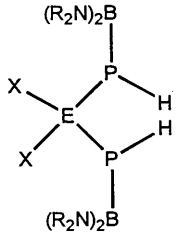

3

2. Experimental

Standard inert atmosphere techniques were used in all synthesis and product manipulations. Solvents were rigorously dried, deoxygenated and distilled prior to use. Mass spectra were obtained from the Midwest Center for Mass Spectrometry, University of Nebraska. Infrared spectra were recorded on a Mattson 2020 FTIR and NMR spectra were obtained from Bruker FX-250 and JEOL-GSX-400 spectrometers. Samples dissolved in a deuterated lock solvent were flame sealed in NMR tubes and referenced externally against Me_4Si (^1H, ^{13}C), and 85% H_3PO_4 (^{31}P). All downfield shifts were assigned $+\delta$s.

2.1. Synthesis of zirconocene bis(borylphosphane) (3a)

A sample of Cp_2ZrCl_2 (1.5 g, 5.1 mmol) (Aldrich) in hexane (40 ml) was cooled to -78°C and solid $LiP(H)B(N^iPr_2)[N(SiMe_3)_2]\cdot DME$ [5] (4.05 g, 10.5 mmol) was added in portions with rapid stirring over 2 h. The mixture was then warmed to 23°C and stirred overnight. The resulting suspension was filtered to remove LiCl, and the filtrate was evaporated to dryness. The red residue was recrystallized from cold hexane leaving red crystalline $Cp_2Zr\{P(H)B(N^iPr_2)\cdot[N(SiMe_3)_2]\}_2$ (**3a**): yield 2.8 g, 66%. Additional product can be harvested from the mother liquor. IR spectrum (KBr, cm^{-1}): 2968(m), 2903(w), 2328(w), 1487(w), 1440(w), 1410(w), 1363(w), 1302(m), 1249(m), 1196(m), 1145(w), 1112(w), 1057(s), 1020(w), 923(s), 885(s), 837(s), 800(m), 742(w), 677(w). ^{31}P-NMR(C_6D_6): δ 37.3 (d, $J_{PH} = 251$Hz). ^1H-NMR(C_6D_6): δ 0.37 (s, 18H, *SiMe*$_3$), 1.26 (d, 6H, $J_{HH} = 7.2$ Hz, C*H*$_3$ (^{i}Pr)), 1.42 (d, 6H, $J_{HH} = 7.2$ Hz, C*H*$_3$ (^{i}Pr)), 2.71 (d, 1H, $J_{PH} = 260$ Hz, P–*H*), 4.40 (sept, 1H, $J_{HH} = 7.1$ Hz, C*H* (^{i}Pr)), 4.74 (sept, 1H, $J_{HH} = 7.1$ Hz, C–*H* (^{i}Pr)), 5.91 (s, 5H, *Cp*). $^{13}C\{^1H\}$(C_6D_6): δ 3.89 (*SiMe*$_3$), 25.28 (*C*H$_3$ (^{i}Pr)), 25.35 (*C*H$_3$(^{i}Pr)), 46.1 (*C*H), 108.2 (*Cp*).

2.2. Formation of complex 4a

Equimolar amounts of **3a** (1.24 g, 1.5 mmol) and $Mo(NBD)(CO)_4$ (0.44 g, 1.5 mmol) (NBD = norbornadiene) were combined in hexane (30 ml) and stirred (6 h). The mixture was vacuum evaporated leaving a red solid that was recrystallized from a minimum of cold hexane (-20°C): yield 0.70 g, 45%. MS (HR-FAB) (*m*/*e*, relative intensity): 1028.2649–1044.2750, 3%, M^+; 271.2, 100%. IR spectrum (KBr, cm^{-1}): 2966(w), 2004(m), 1921(m), 1896(s), 1888(s), 1628(w), 1421(w), 1321(w), 1251(w), 1190(w), 1116(w), 1057(m), 906(w), 883(w), 837(w), 802(w), 729(w). ^{31}P-NMR(C_6D_6): δ 21.4 ($J_{PH} = 285$ Hz). ^1H-NMR(C_6D_6): δ 0.36 (s, Si*Me*$_3$), 1.26 (d, $J_{HH} = 7.2$ Hz, C*H*$_3$(^{i}Pr)), 1.41 (d, $J_{HH} = 7.2$ Hz, C*H*$_3$(^{i}Pr)), 3.5 (d, $J_{PH} = 280$ Hz, P*H*), 4.40 (sept, $J_{HH} = 7.1$ Hz, C*H*(^{i}Pr)), 4.73 (sept, $J_{HH} = 7.1$ Hz, C*H*(^{i}Pr)), 5.90 (s, *Cp*).

2.3. Crystal structure determinations

Suitable crystals of **3a** and **4a** were obtained from recrystallizations from cold hexane. Crystals were mounted in glass capillaries under dry nitrogen and the capillaries were flame sealed. The crystals were centered on a Siemens R3m/V four-circle diffractometer and determinations of the crystal class, orientation matrix and accurate unit cell parameters were made at 20°C. The crystal parameters and data collection details are given in Table 1. Intensity data were collected with Mo–K_α ($\lambda = 0.71073$ Å) monochromated radiation, scintillation counter and pulse height analyzer. Intensities for three standard reflections were monitored every 97 reflections. No sign of crystal decay was noted. All calculations were performed on the Siemens P3 structure solution system using SHELXTL PLUS. Neutral atom scattering factors and anomalous dispersion terms were used for all non-hydrogen atoms. A small empirical adsorption correction was applied in each case by use of ψ-scans. The structures were solved by Patterson techniques and full-matrix least-squares refinements were based on F^2. Anisotropic refinement of **3a** showed that the silyl methyl groups have large U_{iso} values, and the displacements on C(24), C(25), C(27) and C(28) suggest disorder. Further refinement with a disorder model having occupancies C(24)/0.60, C(24′)/0.40; C(25)/0.60, C(25′)/0.40; C(27)/0.56, C(27′)/0.44; C(28)/0.56, C(28′)/0.44 gave slightly lower agreement factors. The final refinement had all ordered non-hydrogen atoms anisotropic, disordered C atoms fixed in occupancies with variable isotropic *U* values, all hydrogen atoms included with ordered H atom positions from the riding model except for the H atoms on the P atoms which were found from the difference maps, and these were allowed to vary in position. H atoms on

the disordered C atoms were fixed in idealized positions The refinement of **4a** was well-behaved. All non-hydrogen atoms refined anisotropically and H atoms were included in idealized positions (riding model) except for the H atoms on the P atoms which were found in the difference maps and their positions allowed to vary.

3. Results and discussion

Group 4 metallo bridged diphosphanes (**5**) containing tertiary phosphorus atoms have been actively studied in part due to their interesting bonding features as well as their ability to act as chelating ligands toward selected metal fragments [9–18]. Analogs containing secondary phosphane centers also have received attention due to their reactivity that in some cases produces metallo-phosphinidenes (**6**), phosphides (**7**) and cyclic species (**8**, **9**) [9,11,18–32]. In all of the previously reported metallo bridged diphosphane compounds, the phosphane substituent groups were organic groups or silyl groups. We have, therefore, been interested in how replacement of these groups by a more electron deficient aminoboryl group might affect the stability, structure and reactivity of the diphosphane.

Table 1
Summary of X-ray data for **3a** and **4a**

	3a	**4a**
Formula	$C_{34}H_{76}B_2N_4P_2Si_4Zr$	$C_{38}H_{76}B_2MoN_4O_4P_2Si_4Zr$
Color	Red	Red
Crystal dimensions (mm)	$0.42\times0.29\times0.11$	$0.14\times0.30\times0.46$
Crystal system	Monoclinic	Triclinic
Space group	$P2_1/c$	$P\bar{1}$
Unit cell dimensions		
a (Å)	15.941(5)	13.067(4)
b (Å)	19.196(5)	15.270(4)
c (Å)	16.639(4)	16.433(5)
α (°)	90	63.20(2)
β (°)	104.38(1)	67.05(2)
γ (°)	90	72.02(2)
V (Å^3)	4932(2)	2659.6(13)
Z	4	2
Formula weight	828.13	1036.11
D_{calc} (g cm^{-3})	1.115	1.294
Adsorption coefficient (mm^{-1})	0.410	0.619
θ Range	1.91–20.00	1.45–25.00
No. of collected reflections	9574	17844
No. of observed reflections	4592	8940
Parameters refined	422	511
R_1 (%) [a]	3.63	3.29
wR_2 (%) [b]	4.99	6.93

[a] $R_1 = \Sigma||F_o|-|F_c||/\Sigma|F_o|$.
[b] $wR_2 = [\Sigma w(|F_o|-|F_c|)]^2/\Sigma[w(F_o^2)^2]^{1/2}$.

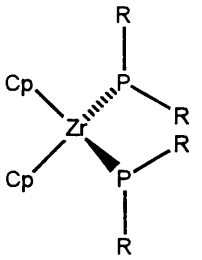

5

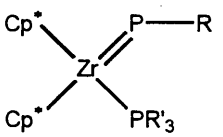

6

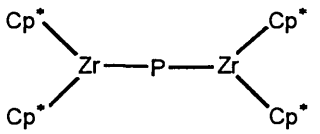

7

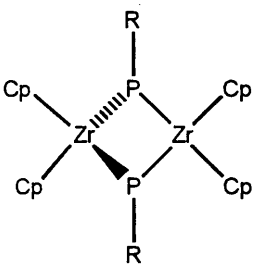

8

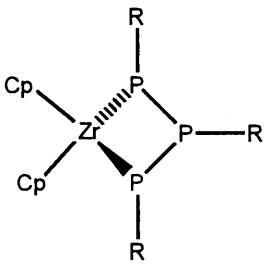

9

Combination of LiP(H)B(N^{i}Pr$_2$)[N(SiMe$_3$)$_2$]·DME with Cp_2ZrCl_2 in a 2:1 ratio in hexane leads to the formation of **3a** (Scheme 1) as a moisture sensitive red crystalline solid. An NMR tube synthesis suggests that the reaction is quantitative, but larger scale syntheses provide yields of only 60–70% due to recrystallization losses brought about by the relatively high solubility in hexane and aromatic solvents. The recrystallization product appears to be better than 95% pure, as indicated by ^{31}P- and ^{1}H-NMR analyses; however, a small impurity of the starting phosphane (**10**) (^{31}P δ −184.9) has proved difficult to remove completely. Attempts were made to record FAB-mass spectra for **3a**, but they showed no evidence for the parent ion, M^+, or other high mass ions (Scheme 1). Only low mass ions typical of the borylphosphane and Cp_2Zr fragments were detected. An IR spectrum of **3a** shows a weak P–H absorption at 2328 cm^{-1} that is shifted up-frequency from the PH_2 absorption in **10**, 2276 cm^{-1}. NMR spectra are completely consistent with the formation of the proposed zirconocene diphosphane. In particular, the ^{31}P{^{1}H}-NMR spectrum shows a singlet at δ 37.3 that has

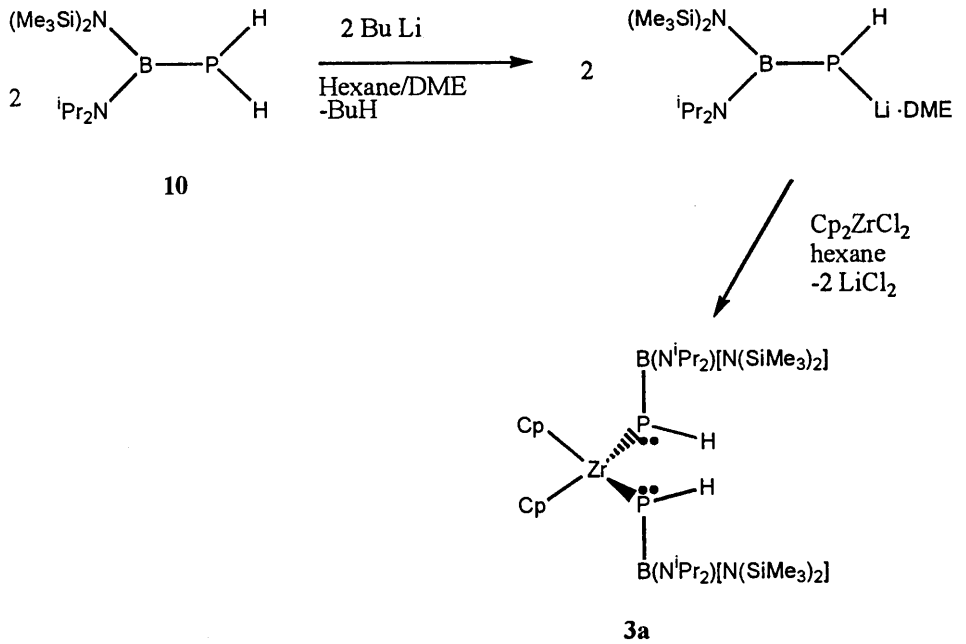

Scheme 1.

a first-order doublet pattern, $J_{PH} = 251$ Hz, in the proton coupled spectrum. This resonance is shifted dramatically downfield from the resonance in **10** (triplet, δ −184.9, $J_{PH} = 210.9$ Hz) and its lithium salt LiP(H)B(N^{i}Pr$_2$)[N(SiMe$_3$)$_2$]·DME (doublet, δ −183.2, $J_{PH} = 163.8$ Hz). The ^{1}H- and ^{13}C{^{1}H}-NMR spectra for **3a** show single resonances for the Me$_3$Si and Cp groups, and this observation indicates that **3a** exists in solution as a *rac* isomer or as a *rac*/*meso* isomer mixture undergoing rapid exchange by rotation about the Zr–P bonds. In addition, the ^{1}H- and ^{13}C{^{1}H}-NMR spectra show two resonances for the ^{i}Pr methyl groups consistent with methyl group inequivalence expected for planar BN^{i}Pr$_2$ aminoboryl fragments. The methine protons also produce two resonances in the ^{1}H-NMR spectrum, but only one resonance is resolved in the ^{13}C{^{1}H}-NMR spectrum. Finally, the ^{1}H-NMR spectrum contains a single resonance for the P–H groups, δ 3.5, that is split into a doublet, $J_{PH} = 280$ Hz.

Geoffroy [10], Baker [13,14,16] and Stephan [17] have examined the chelating properties of several Cp$_2$Hf(PR$_2$)$_2$ and Cp$_2$Zr(PR$_2$)$_2$ metallo-bridged diphosphanes, containing tertiary phosphane donor fragments (R = Et, Cy, Ph), toward electron-rich metal fragments including Mo(CO)$_4$, W(CO)$_4$, Fe(CO)$_3$, Rh (indenyl), Ni(COD), Pd(PPh$_3$)$_2$ and Pt(PPh$_3$)$_2$. In a similar fashion Hey–Hawkins [32] has reported formation of complexes with the chelating *sec*-diphosphane Cp$_2$Zr-[P(H)(2,4,6-^{i}Pr$_3$C$_6$H$_2$)]$_2$ on Cr(CO)$_4$ and Mo(CO)$_4$. Molecular structure determinations for the bimetallic complexes Cp$_2$Zr(μ-PPh$_2$)$_2$·W(CO)$_4$ (**11**) [10], Cp$_2$Zr(μ-PPh$_2$)$_2$·Mo(CO)$_4$ (**12**) [17], Cp$_2$Hf(μ-PEt$_2$)$_2$·Mo(CO)$_4$ (**13**) [13], Cp$_2$Zr(μ-PPh$_2$)$_2$·Rh(η^5-indenyl) (**14**) [14], Cp$_2$Hf(μ-PPh$_2$)$_2$·Pd(PPh$_3$) (**15**) [16] and Cp$_2$Hf(μ-PPh$_2$)$_2$·Rh(H)(CO)(PPh$_3$) (**16**) [19] and the heterotrimetallic complex Cp$_2$Zr(μ-PEt$_2$)$_2$·Ni(μ-PEt$_2$)$_2$ HfCp$_2$ (**17**) [16] have been determined. Compounds **11**–**14**, **16** and **17** have planar MP$_2$M′ rings while **15** displays a folded HfP$_2$Pd ring ($\varnothing = 24.49°$). Baker has completed EHMO analyses for the chelating metallo diphosphane model compound, Cp$_2$Zr(PH$_2$)$_2$ [16], and these results provide a clear view on how the fragment acts as a chelating ligand. The Cp$_2$Zr(PH$_2$)$_2$ fragment provides two filled donor MOs that are largely localized on the phosphorus atoms. The lower energy MO (1a$_1$) is an in-phase combination of sp$_x$p$_z$ hybrids. An out-of-phase combination (1b$_1$) of sp$_x$p$_z$ hybrids appears at slightly higher energy. The latter is the HOMO for the idealized fragment. These MOs can combine with empty 2a$_1$ and 1b$_1$ MOs on the Mo(CO)$_4$ fragment giving rise to the observed *cis*-L$_2$Mo(CO)$_4$ complex. The Mo(CO)$_4$ fragment also possesses a HOMO (1a$_1$) that is appropriately positioned to interact with the LUMO (2a$_1$) of the Cp$_2$Zr(PH$_2$)$_2$ fragment. If effective, this overlap results in a σ symmetry Mo → Zr bond. Indeed, with selected electron rich Pt(0) and Rh(I) fragments, this type of M → Zr σ bond overlap appears. However, Baker points out that the 1a$_1$ HOMO of Mo(CO)$_4$ is contracted by competitive π-backbonding with the CO ligands. This in turn makes the Mo(CO)$_4$ a poor σ donor along the *z* axis bisecting the two *cis* positions occupied by the phosphane donor centers.

The question that remains to be addressed is: Does replacement of the organic substituents on a metallo *sec*-diphosphane by an electron withdrawing group such as an aminoboryl group change its chelation properties?

Combination of **3a** with $Mo(CO)_4(NBD)$ in hexane gives a very soluble red complex **4a** that deposits red crystals upon standing at -20°C. The complexation chemistry is summarized in Eq. (2).

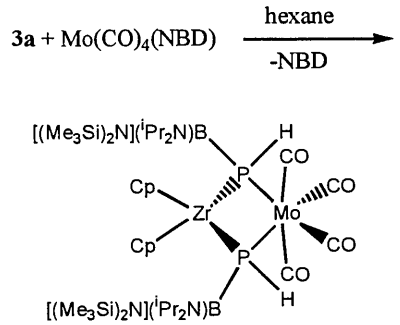

4a (2)

The complex **4a** displays a parent ion envelop in its HRFAB-MS: *m*/*e* 1044.2750–1028.2649 (15 peaks: 1036.2732, 100% abundant). The calculated masses and isotopic intensity pattern for the expected bimetallic complex agree very closely with the observed pattern. The IR spectrum of **4a** is similar to that shown by **3a** except that there are four prominent new absorbances at 2004, 1921, 1896 and 1888 cm^{-1}. A *cis*-$L_2M(CO)_4$ complex is predicted, from group theoretical analysis, to show four (**2a**, $+b_1+b_2$) terminal CO stretching frequencies [35] and the observed band positions are typical of bis-phosphane complexes that contain *sec*-organo phosphane donor groups [36]. The $^{31}P\{^1H\}$-NMR spectrum shows a single resonance at δ 21.4 shifted upfield from the ligand **3a**. Restoration of the proton–phosphorus coupling gives rise to the expected doublet pattern, $^1J_{PH} = 285$ Hz. The ^{1}H- and $^{13}C\{^1H\}$-NMR spectra for **4a** show single resonances for both the Me_3Si and Cp groups. In this case, the single environment for the Cp groups requires that **4a** exists as the *rac* isomer in solution since coordination of the two phosphorus atoms to the $Mo(CO)_4$ fragment prohibits potential Zr–P bond rotation. The ^{1}H-NMR spectrum also shows a single resonance, δ 2.7, for the P–H group that is split into a doublet, $J_{PH} = 280$ Hz.

The molecular structures of the ligand **3a** and complex **4a** were determined by single crystal X-ray diffraction methods. Views of the molecules are shown in Figs. 1 and 2, respectively. As shown in Fig. 3, **3a** has a 'close twofold axis' that passes through the Zr atom; however, this is not a crystallographic symmetry element. The Zr atom is pseudo-tetrahedral with P(1)–Zr–P(2) 96.68(5)° and X(1)–Zr–X(2) 127.2(2)° (Table 2). The more open angle involving the Cp ring centroids probably reflects the larger Cp···Cp repulsions. Interestingly, the Zr–P(1) distance, 2.596(2) Å, is shorter than the Zr–P(2) distance, 2.627(2) Å. Given the small bond length e.s.d. values this difference, 0.031 Å, appears to be significant. By comparison, molecular structure determinations for $Cp_2Hf(PEt_2)_2$ (Hf–P 2.488(1), 2.682(1) Å) [12], $Cp_2Hf[P(SiMe_3)_2]_2$ (Hf–P 2.553(1), 2.654(1) Å) [37] and $[(Me_3Si)_2C_5H_3)]_2$ $Zr[1,2\text{-}(PPh_2)_2C_6H_4]$ (Zr–P 2.560(4), 2.647(6) Å) [38] show even larger M–P bond distance variations. These compounds also display a planar or near-planar geometry for the phosphorus atom associated with the shorter distance. The second P atom has a more pyramidal geometry. These observations have led to the suggestion that the bonding in these compounds is best represented by the valence bond representation summarized by **18**.

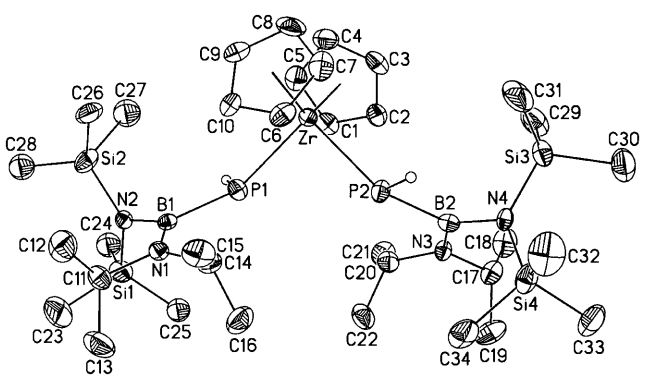

Fig. 1. Molecular structure and atom labeling scheme for $Cp_2Zr\{P(H)B(N^iPr_2)[N(SiMe_3)_2]\}_2$ (**3a**) (20% thermal ellipsoids).

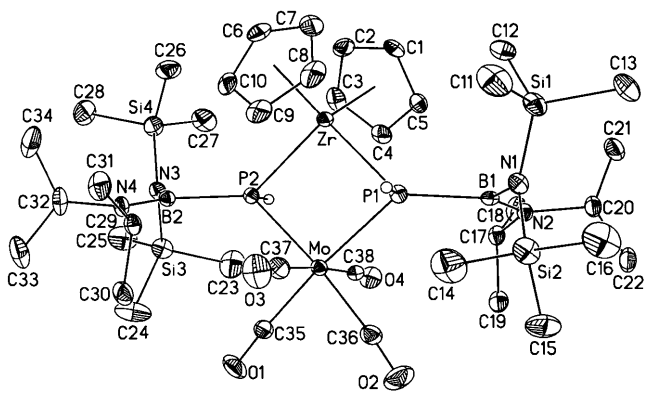

Fig. 2. Molecular structure and atom labeling scheme for $Cp_2Zr\{P(H)B(N^iPr_2)[N(SiMe_3)_2]\}_2{\cdot}Mo(CO)_4$ (**4a**) (30% thermal ellipsoids).

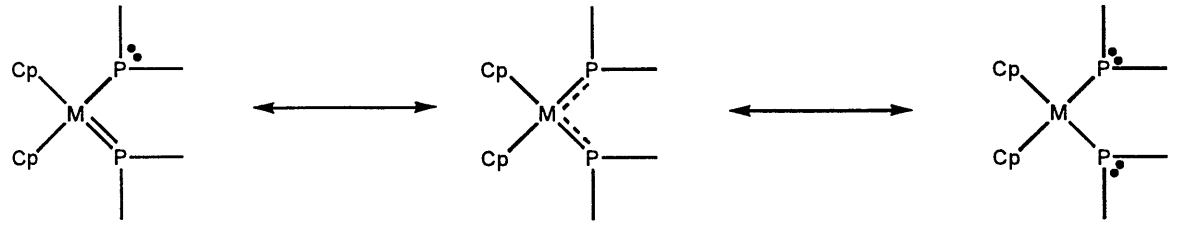

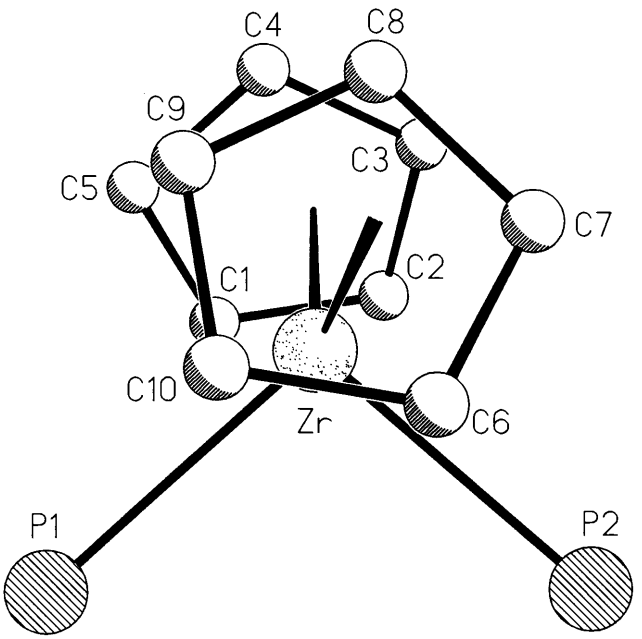

Fig. 3. View of the central Zr atom coordination geometry in **3a**.

In contrast, the analog $Cp_2Zr[P(H)(2,4,6\text{-}^tBu_3C_6H_2)]_2$ displays equal Zr–P distances (Zr–P 2.681(5), 2.682(5) Å) with one near planar P atom and one pyramidal P atom [9,33]. The compound $(MeC_5H_4)_2Zr[P(SiMe_3)_2)]_2$ has a Zr–P distance differential similar to **3a** (Zr–P 2.600(2), 2.634(2) Å) with *both* P atoms in near-planar environments [34]. For comparison, it is important to assess the geometry about P(1) and P(2) in **3a**. The H atom on each P atom was located in difference Fourier maps after refining all non-hydrogen atoms anisotropically, and the positions were varied during the final refinements. It is interesting that *both* P(1) and P(2) in **3a** are *pyramidal* (sum of angles: 346.6(2)°, 341.3(2)°), although these angles fall in-between the typically reported planar (350–360°) and pyramidal (321–336°) angle ranges in the complexes listed above. This sug-

Table 2
Selected bond distances (Å) and angles (°) for **3a** and **4a**

	3a		**4a**	
Zr–C $(Cp)_{avg}$	Zr–C	2.509(6)	Zr–C	2.514(4)
Zr–P	Zr–P(1)	2.596(2)	Zr–P(1)	2.635(1)
	Zr–P(2)	2.627(2)	Zr–P(2)	2.629(1)
B–P	B(1)–P(1)	1.916(7)	B(1)–P(1)	1.981(4)
	B(2)–P(2)	1.926(6)	B(2)–P(2)	1.988(4)
B–N	B(1)–N(1)	1.407(6)	B(1)–N(1)	1.491(5)
	B(1)–N(2)	1.487(7)	B(1)–N(2)	1.393(5)
	B(2)–N(3)	1.422(7)	B(2)–N(3)	1.488(5)
	B(2)–N(4)	1.469(7)	B(2)–N(4)	1.391(5)
Si–N	Si(1)–N(2)	1.732(4)	Si(1)–N(1)	1.735(3)
	Si(2)–N(2)	1.727(4)	Si(2)–N(1)	1.765(3)
	Si(3)–N(4)	1.743(4)	Si(3)–N(3)	1.757(3)
	Si(4)–N(4)	1.725(4)	Si(4)–N(3)	1.738(3)
Mo–P			Mo–P(1)	2.583(1)
			Mo–P(2)	2.586(1)
Mo–CO			Mo–C(35)	1.982(4)
			Mo–C(36)	1.976(5)
			Mo–C(37)	2.027(4)
			Mo–C(38)	2.041(4)
Mo···Zr			Mo···Zr	3.343(1)
P–Zr–P	P(1)–Zr–P(2)	96.68(5)	P(1)–Zr–P(2)	99.04(4)
X [a]–Zr–P	X(1)–Zr–P(1)	105.5(2)	X(1)–Zr–P(1)	106.4(4)
	X(2)–Zr–P(2)	100.2(2)	X(2)–Zr–P(2)	106.3(4)
	X(1)–Zr–P(2)	106.0(2)	X(1)–Zr–P(2)	106.3(4)
	X(2)–Zr–P(1)	116.0(2)	X(2)–Zr–P(1)	106.6(4)
X–Zr–X	X(1)–Zr–X(2)	127.2(2)	X(1)–Zr–X(2)	128.5

[a] X corresponds to the vector connecting the Zr atom to the centroid of the Cp rings.

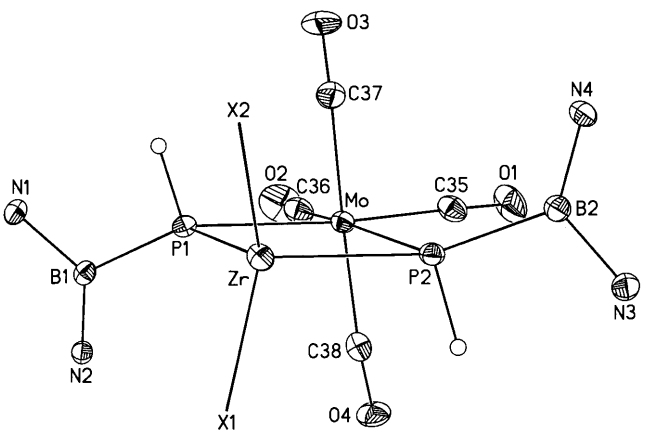

Fig. 4. View of central ZrP_2Mo core in **4a**.

gests that **3a** has a structure like that represented by **18″**. Although not yet entirely demonstrated, it appears that steric effects play an important role in determining the structural condition adopted by any individual compound along the **18**–**18′**–**18″** continuum. The P–B bond distances fall in the range expected for single bond distances [2]. The boron and nitrogen atoms are trigonal planar and each boron has a long and a short B–N distance with the longer distance belonging to the $B–N(SiMe_3)_2$ groups and the shorter distance associated with the $B–N^iPr_2$ groups. Similar features have been seen in several aminoboryl phosphanes [2,5].

The structure analysis of **4a** shows that the general geometrical configuration of **3a** changes little with bonding to the $Mo(CO)_4$ fragment. The central ZrP_2Mo four-membered ring is planar with the P–H bonds *trans* to each other as shown in Fig. 4. The two Zr–P bond lengths are now nearly the same (Zr–P(1) 2.635(1) Å, Zr–P(2) 2.629(1) Å) and slightly elongated compared to the short distance in **3a**. They are unchanged from the long distance in **3a**. In contrast, there are short and long Zr–P distances in $Cp_2Zr(PPh_2)_2W(CO)_4$ (2.619(3) and 2.631(3) Å) [10]. The two Mo–P distances in **4a** (2.583(1) and 2.586(1) Å) are identical and slightly longer than the average Mo–P distances in $Cp_2Hf(PEt_2)_2{\cdot}Mo(CO)_4$ (2.536(1) Å) [13] and in *cis*-$[Ph(H)_2P]_2Mo(CO)_4$ (2.508(3) Å) [36]. The internal P(1)–Zr–P(2) angle, 99.04(4)°, is only slightly enlarged from the angle in **3a**. The non-bonded Mo···Zr distance, 3.343(1) Å, is long and can be compared with the Mo···Zr separation (3.299(1) Å) in $Cp_2Zr(PPh_2)_2{\cdot}Mo(CO)_4$ [17], the W···Zr separation (3.289(1) Å) in $Cp_2Zr(PPh_2)_2W(CO)_4$ [10] and the Mo···Hf distance (3.400(1) Å) in $Cp_2Hf(PEt_2)_2Mo(CO)_4$ [13]. The Mo atom has an octahedral *cis*-$L_2M(CO)_4$ geometry with the Mo–CO bonds *trans* to P(1) and P(2) (average 1.979(5) Å) shorter than the *cis* M–CO distances (average 2.034(4) Å). This is typical of *cis*-$L_2M(CO)_4$ complexes where L = phosphanes that are stronger σ donors and weaker π acceptors than CO. The *exo* $B(N^iPr_2)[N(SiMe_3)_2]$ groups form planes that are rotated approximately perpendicular to the P_2Mo plane. The P–B distances are significantly elongated (average 1.984(4) Å) relative to the distances in **3a** indicative of the increased phosphorus atom coordination number. As noted in **3a** the B–N bond lengths fall into two groups: short $B–N^iPr_2$ distances and long $B–N(SiMe_3)_2$ distances.

4. Conclusion

Part of the intent in studying the formation of **3a** was to determine if the aminoboryl substituents on the phosphane would convey different chemistry on the metallo diphosphanes $Cp_2Zr(PR_2)_2$ compared to those known examples where R = organyl or silyl. On first blush, it seems that there is not a large structural or electronic modification although it appears that **3a** does not adopt the typical single Zr–P/double Zr=P bond structure idealized in **18**. Further, the coordination chemistry of **3a** toward $Mo(CO)_4$ is not unexpected. Nonetheless, it is anticipated that the fragile nature of the *exo*-P–B bonds in **3a** and **4a** compared to the P–C bonds in organyl derivatives will make the chemistry of **3a** and **4a** more exciting, and aspects of that chemistry will be examined in the future.

5. Supplementary material

Crystallographic data for the structures reported in this paper have been deposited with the Cambridge Crystallographic Data Centre, CCDC no.139157 for **3a** and CCDC no. 139158 for **4a.** Copies of this information may be obtained free of charge from the Director, CCDC, 12 Union Road, Cambridge, CB2 1EZ, UK (fax: +44-1223-336-033; e-mail: deposit@ccdc.cam.ac.uk or http://www.ccdc.cam.ac.uk).

Acknowledgements

Financial support for this work was provided by the National Science Foundation, Grant CHE-9508668.

References

[1] A.D. Norman, in: J.J. Zuckerman (Ed.), Inorganic Reactions and Methods, vol. 2, VCH, Deerfield Beach, FL, 1987.
[2] R.T. Paine, H. Nöth, Chem. Rev. 95 (1995) 343.
[3] D. Dou, M. Westerhausen, G.L. Wood, G. Linti, E.N. Duesler, H. Nöth, R.T. Paine, Chem. Ber. 126 (1993) 379.
[4] D. Dou, G.W. Linti, T. Chen, E.N. Duesler, R.T. Paine, H. Nöth, Inorg. Chem. 35 (1996) 3626.
[5] D. Dou, M. Fan, E.N. Duesler, H. Nöth, R.T. Paine, Inorg. Chem. 33 (1994) 2151.
[6] P. Kölle, Ph.D. Dissertation, University of Munich, 1987.
[7] G.W. Linti, Ph.D. Dissertation, University of Munich, 1990.
[8] T. Chen, J. Jackson, S.A. Jasper, E.N. Duesler, H. Nöth, R.T. Paine, J. Organomet. Chem. 582 (1999) 25.
[9] E. Hey-Hawkins, Chem. Rev. 94 (1994) 1661 and references therein.
[10] T.S. Targos, R.P. Roseu, R.R. Whittle, G.R. Geoffroy, Inorg. Chem. 24 (1985) 1375.
[11] R.T. Baker, P.J. Krusic, T.H. Tulip, J.C. Calabrese, S.S. Wreford, J. Am. Chem. Soc. 105 (1983) 6763.
[12] R.T. Baker, J.F. Whitney, S.S. Wreford, Organometallics 2 (1983) 1049.
[13] R.T. Baker, T.H. Tulip, S.S. Wreford, Inorg. Chem. 24 (1985) 1379.
[14] R.T. Baker, T.H. Tulip, Organometallics 5 (1986) 839.
[15] R.T. Baker, J.C. Calabrese, T.E. Glassman, Organometallics 7 (1988) 1889.
[16] R.T. Baker, W.C. Fultz, T.B. Marder, I.D. Williams, Organometallics 9 (1990) 2357.

[17] L. Gelmini, L. Matasso, D.W. Stephan, Inorg. Chem. 24 (1985) 2585.
[18] L. Gelmini, D.W. Stephan, Inorg. Chim. Acta 111 (1986) L17.
[19] L. Gelmini, D.W. Stephan, Organometallics 7 (1988) 839.
[20] B.L. Benac, R.A. Jones, Polyhedron 8 (1989) 1774.
[21] Z. Hou, D.W. Stephan, J. Am. Chem. Soc. 114 (1992) 10088.
[22] J. Ho, R.J. Drake, D.W. Stephan, J. Am. Chem. Soc. 115 (1993) 3792.
[23] Z. Hou, T.L. Breen, D.W. Stephan, Organometallics 12 (1993) 3158.
[24] J. Ho, Z. Hou, R.J. Drake, D.W. Stephan, Organometallics 12 (1993) 3145.
[25] J. Ho, R. Rousseau, D.W. Stephan, Organometallics 13 (1994) 1918.
[26] M.C. Fermin, J. Ho, D.W. Stephan, J. Am. Chem. Soc. 116 (1994) 6033.
[27] M.C. Fermin, J. Ho, D.W. Stephan, Organometallics 14 (1995) 4247.
[28] T.L. Breen, D.W. Stephan, J. Am. Chem. Soc. 118 (1996) 4204.
[29] E. Hey, S.G. Bott, J.L. Atwood, Chem. Ber. 121 (1988) 561.
[30] E. Hey, J. Organomet. Chem. 378 (1989) 375.
[31] E. Hey, U. Müller, Z. Naturforsch 44b (1989) 1538.
[32] E. Hey-Hawkins, F. Lindenberg, Chem. Ber. 125 (1992) 1815.
[33] E. Hey-Hawkins, S. Kurz, J. Organomet. Chem. 479 (1994) 125.
[34] U. Senff, S. Kurz, E. Hey-Hawkins, Z. Anorg. Allgem. Chem. 623 (1997) 1255.
[35] K.F. Purcell, J.C. Kotz, Inorganic Chemistry, W.B. Saunders Co, New York, 1977, p. 901.
[36] T. Campbell, A.M. Gibson, R. Hart, S.D. Orchard, S.J.A. Pope, G. Reid, J. Organomet. Chem. 592 (1999) 296 and references therein.
[37] L. Weber, G. Meine, R. Boese, N. Augart, Organometallics 6 (1987) 2484.
[38] R. Bohra, P.B. Hitchcock, M.F. Lappert, W.P. Leung, J. Chem. Soc. Chem. Commun. (1989) 728.